PCCP

Accepted Manuscript

ROYAL SOCIETY OF CHEMISTRY

www.rsc.org/pccp

PCCP

PAPER

Self-deposition of Pt Nanoparticles on Graphene Woven Fabrics for Enhanced Hybrid Schottky Junction and Photoelectrochemical Solar Cells

Received 00th January 20xx,
Accepted 00th January 20xx

DOI: 10.1039/x0xx00000x

www.rsc.org/

Zhe Kang[a,b,c], Xinyu Tan[a*], Xiao Li[c], Ting Xiao[a], Li Zhang[c], Junchao Lao[d], Xinming Li[e], Shan Cheng[b], Dan Xie[f], Hongwei Zhu[c*]

In this work, we demonstrated a self-deposition method to deposit Pt nanoparticles (NPs) on graphene woven fabrics (GWF) to improve the performance of graphene-on-silicon solar cells. The deposition of Pt NPs increased the work function of GWF and reduced the sheet resistance of GWF, thereby improving the power conversion efficiency (PCE) of graphene-on-silicon solar cells. The PCE (>10%) was further enhanced via solid electrolyte coating on the hybrid Schottky junction in photoelectrochemical solar cells. These results suggest that the combination of self-deposition of Pt NPs and solid-state electrolyte coating on graphene-on-silicon is a promising way to produce high performance graphene-on-semiconductor solar cells.

Introduction

Two-dimensional graphene (Gr) has attracted tremendous attention because of its unique electronic, thermal, mechanical, and optical properties and many potential applications.[1-3] Transferring Gr onto silicon produces a Schottky junction, which can operate as a solar cell under illumination.[4] In recent years, there is a growing interest in applying Gr in the n-type silicon Schottky junction to produce Gr/n-Si solar cells.[5-10] Gr/n-Si solar cells can avoid the complex fabrication process compared to traditional Si solar cells. However, the devices based on the pristine Gr only showed a maximum power conversion efficiency (PCE) less than 6%.[11, 12] The low PCE is caused by the low work function and imperfect conductivity of pristine Gr, as well as the high carrier recombination rate at the Gr/n-Si interface.[9, 13, 14]

Recently, various approaches have been employed to improve the efficiency of Gr/Si solar cells. These efforts include altering the network structure (incorporation of Gr woven fabrics (GWF),[15,16] deposition of Au nanoparticles (NPs) on Gr,[17] chemical doping of Gr,[18]), controlling the number of layers of Gr,[6,19] controlling the thickness of the interfacial oxide at the Gr/n-Si interface,[20] using Si nanostructure arrays to enhance light absorption,[16,21-23] engineering the Gr/n-Si interface,[22,24] as well as applying an antireflection coating.[4,5] Among them, deposition of Au NPs on Gr (Au-Gr) is one of the most popular methods which offer the opportunity to not only control the work function of graphene but also improve its electrical conductivity.[9, 25] The PCE of solar cells with Au-Gr on n-type silicon (Au-Gr/n-Si) can reach 7.36%.[17] However, further improvement of the PCE is limited by the reduced light transmittance caused by Au NPs.[17] As Pt has a higher work function than that of Au, the surface properties of GWF can be properly turned by less Pt NPs than Au NPs. Traditional methods to deposit Pt NPs on graphene usually require complicated procedures,[26] limiting the application of Pt NPs in solar cells.

Herein, we aimed to develop a self-deposition method for in situ galvanic synthesis of Pt NPs on GWF to generate Pt-GWF. We report the development of high-efficiency GWF/n-Si Schottky junction solar cells by depositing Pt NPs on GWF and decorating GWF with embedded solid electrolyte. Pt NPs deposition on GWF resulted in p-type doping of graphene, and was shown to be an effective approach to achieve high work function and enhanced electrical conductivity of graphene, compared to other approaches. A maximum PCE of 7.94% was achieved for n-type silicon solar cells with Pt-GWF (Pt-GWF/n-Si). The PCE of Pt-GWF/n-Si was further enhanced to 10.02% by decoration of solid electrolyte on Pt-GWF/n-Si.

Experimental

[a] Hubei Provincial Collaborative Innovation Center for New Energy Microgrid, China Three Gorges University, Yichang 443002, China. Email: husttanxin@tsinghua.edu.cn
[b] College of Electrical Engineering & New Energy, China Three Gorges University, Yichang 443002, China.
[c] School of Materials Science and Engineering, Tsinghua University, Beijing 100084, China. Email: hongweizhu@mail.tsinghua.edu.cn
[d] Department of Physics, and Institute for Advanced Study, Nanchang University, Nanchang 330031, China
[e] National Center for Nanoscience and Technology, Beijing 100190, China
[f] Tsinghua National Laboratory for Information Science and Technology, and Institute of Microelectronics, Tsinghua University, Beijing 100084, China

Electronic Supplementary Information (ESI) available: [details of any supplementary information available should be included here]. See DOI: 10.1039/x0xx00000x

Preparation of GWF.

GWF was generated using atmospheric pressure chemical vapor deposition (APCVD) with a copper mesh as the substrate. The copper mesh was cut into a proper size and rinsed with hydrochloric acid and ethyl-alcohol to remove the surface oxide layer and contaminants. Then it was placed into a quartz tube in a CVD reactor. The CVD reactor was heated up to 1000 °C at 10 °C min^{-1} under Ar (300 mL min^{-1}) and H_2 (45 mL min^{-1}). Afterwards, the flow of H_2 was switched off and the flow rate of Ar was set to 200 mL min^{-1}. CH_4 was introduced at 20 mL min^{-1} for 15 min. Finally, the mesh was quickly cooled down to room temperature. After etching the copper mesh away with a $FeCl_3$/HCl solution ($FeCl_3$: 1 mol/L; HCl: 0.5 mol/L), the GWF was obtained. The GWF was further rinsed by deionized (DI) water for 4 h to completely remove the residual ions.

Assembly of the GWF/n-Si Solar Cells.

Single crystal n-type silicon (400 μm, 2-4 Ω cm) with a 300 nm thick patterned SiO_2 surface layer was used as the solar cell substrate. The substrate was rinsed by acetone to remove organic impurities. The top side had a 0.11 cm^2 Si window. The bottom side was coated with Ti (10 nm)/Au (50 nm) through e-beam evaporation. Then the prepared GWF was transferred on the substrate to generate the GWF/n-Si solar cells. Au wires were connected to the surface of the GWF with silver paint.

Self-deposition of Pt NPs.

The positive (GWF) and negative (n-Si) electrodes of the GWF/n-Si solar cell was connected by a conducting wire. Chloroplatinic acid solution (10 mM) was added on the Si window on the GWF/n-Si solar cell, followed by illumination at 82 mW cm^{-2} for 3-15 min using a solar simulator. After illuminating, the remaining chloroplatinic acid solution on the solar cell was removed.

Preparation and Spin-coating of Solid Electrolytes.

Polyvinyl alcohol (PVA) (0.5 g) was added in DI water (10 mL) under stirring. The solution was then heated up to 75 ^{o}C till PVA was completely dissolved. The PVA and nitric acid (PVA+HNO_3) solid electrolyte was obtained by further adding 0.97 g 1 M HNO_3 (mass fraction: 65%~68%) solution into the PVA gel at room temperature. To make a hybrid solar cell, the solid electrolyte was spin-coated on Pt-GWF/Si at 5000 rpm for 60 s.

Characterizations.

A Newport 69907 solar simulator was used to measure the photovoltaic properties of the solar cells under AM 1.5. The illumination intensity was calibrated to 82 mW cm^{-2}. A Keithley 2601A SourceMeter was used to collect current-voltage (I-V) data. A scanning electron microscope (SEM, LEO 1530, 5 kV) and a transmission electron microscope (TEM, JEM-2010, 120-200 kV) were used for morphology and structure characterizations. A Raman spectroscope (Renishaw, RM2000, He-Ne laser excitation at 514 nm) was used for structure characterization. An Agient Carry 5000 spectrophotometer was used for transmittance measurement. Ultraviolet photoelectron spectroscopy (UPS) and X-ray photoelectron spectroscopy (XPS) (Thermo Fisher, ESCALAB 250Xi) were employed for the work function measurement and elemental content analysis.

Results and discussion

GWF was transferred on n-Si to produce GWF/n-Si solar cells (Fig. 1a). The PCE of pristine GWF/n-Si solar cells is 3~5%. In order to deposit Pt NPs on GWF, chloroplatinic acid was added on the Si window on the pristine GWF/n-Si solar cells (Fig. 1b). A conducting wire was used to connect the GWF and n-Si. Then a solar simulator illuminated the device to deposit Pt on GWF. This self-deposition approach realized in situ galvanic synthesis of Pt-GWF on silicon wafer by depositing Pt NPs directly on GWF, combining the photo-assisted deposition (PAD) method[27] and the electrochemical deposition method[28].

In this process, electrons were exported from n-Si. The conducting wire transferred the electrons to chloroplatinic acid, enabling a series of reduction reactions of $[PtCl_6]^{2-}$ to $[PtCl_4]^{2-}$, and eventually to Pt[28]. This self-deposition approach does not need complex procedures to prepare Pt NPs[29] nor requires a metal substrate as the sacrificial layer to provide electrons for depositing Pt NPs[30], thereby avoiding defects on Pt-GWF. Fig. 1c shows the schematic diagram of Pt-GWF/n-Si solar cells with Pt NPs deposited on the surface of GWF.

As shown in Fig. 2, Sample A and B represent the pristine GWF/n-Si solar cells. Sample C is the Pt-GWF/n-Si solar cell generated by photo-assisted deposition of Pt NPs on Sample A (10 min deposition time). The photo-assisted deposition method[27] is similar to the self-deposition method but without the conducting wire. Sample D is Pt-GWF/Si generated by the self-deposition approach on Sample B (10 min deposition time). The PCE of Sample C was enhanced from 4.23% to 6.87% (Fig. 2a).The PCE of Sample D was improved from 4.10% to 7.94%. As shown in Fig. 2 and Fig. S1, the Pt-GWF/n-Si deposited with Pt NPs by self-deposition has higher PCE comparing to Pt-GWF/n-Si assembled by photo-assisted deposition with the same deposition time of 10 min. Moreover, the PCE of 7.94% is higher

PCCP

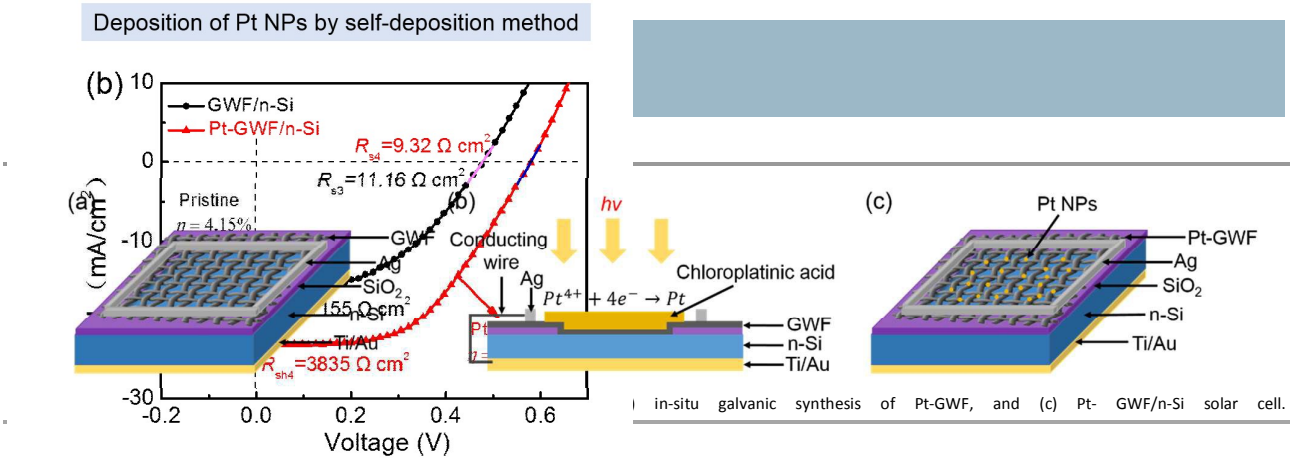

in-situ galvanic synthesis of Pt-GWF, and (c) Pt- GWF/n-Si solar cell.

than the previously reported PCE (7.36%) obtained by Au NPs doping on graphene.[17]

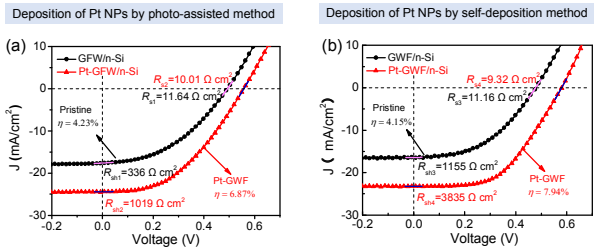

Figure 2. (a) J-V curves of pristine GWF/n-Si solar cells (black, Sample A) and Pt-GWF/n-Si solar cells (red, Sample C). (b) J-V curves of pristine GWF/n-Si solar cells (black, Sample B) and Pt-GWF/n-Si solar cells (red, Sample D).

As shown in Table S1, the series resistance (R_s) of the solar cell dropped from 11.6 to 10.0 Ω cm^2 for Sample C, and from 11.2 to 9.3 Ω cm^2 for Sample D, while the shunt resistance (R_{sh}) of the solar cell increased from 336 to 1019 Ω cm^2 for Sample C and from 1155 to 3835 Ω cm^2 to Sample D, respectively. The decrease of R_s and the increase of R_{sh} contributed to the improvement of the PCE.[17] Pt NPs improved both the open circuit voltage (V_{oc}) and short circuit current density (J_{sc}) of the solar cells. Under the same condition of Pt NPs deposition, the self-deposition method (Sample D) is superior to the photo-assisted deposition method (Sample C).

There are three reasons that caused the enhancement of the PCEs of solar cells: i) the Pt NPs improved the work function of GWF and thus resulted in an enhanced built-in electric field with increased V_{oc} and R_{sh}; ii) the Pt NPs reduced the sheet resistance of GWF and led to an increase in J_{sc} and a decrease in R_s; iii) the metal was placed close to the interface between two dielectrics (air and GWF/n-Si interface), in which case light scattered preferentially into the dielectric with a larger permittivity, i.e., the GWF/n-Si interface. The scattered light then acquired an angular spread in the GWF/n-Si interface, causing an increase in the optical path length.[31] As a result, the incident light was better absorbed by n-Si to produce more photocarriers.

To investigate the structural and morphological changes of GWF/n-Si solar cells after the deposition of Pt NPs, a comparative study was performed on pristine GWF and Pt GWF. Top-view optical images and SEM images of GWF/n-Si and Pt-GWF/n-Si solar cells are shown in Fig. S2. Since Pt NPs were too small to be observed (Fig. 3a), TEM was used to identify the Pt NPs (Fig. 3b). The distance between the adjacent lattice fringes was 0.225 nm, corresponding to the interplanar space of the {111} plane of the face-centered cubic modification by Pt.[32]

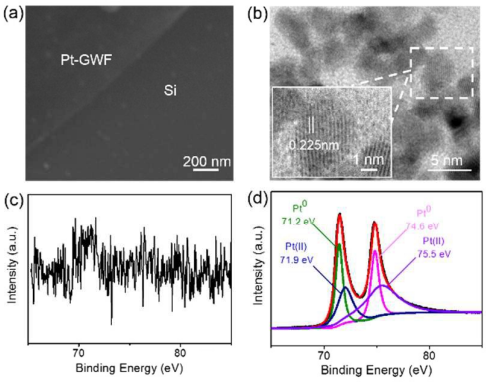

Figure 3. (a) SEM image of Pt-GWF on silicon. (b) TEM image of Pt-GWF. The insets show the magnified view of the selected region (c) XPS spectrum of GWF. (d) XPS spectrum of Pt-GWF. The black and red curves represent the experimental measurement and fitting result, respectively.

XPS spectra were collected to measure the content of Pt NPs on GWF. Fig. 3c shows the XPS spectrum of pristine GWF and Fig. 3d shows the XPS spectrum of Pt-GWF deposited with Pt NPs. The atomic ratio of Pt is 0.5%. The major peaks at 71.2

and 74.6 eV in Fig. 3d can be assigned to the zero valence state of Pt. In addition, the peak at 74.6 eV may be attributed to the interaction between Pt NPs and graphene.[33]

The relationship between the deposition time and the performance of Pt-GWF/n-Si solar cells was investigated. As shown in Fig. 4a, the solar cells deposited with Pt NPs for 10 to 15 min showed higher PCEs than those of the cells deposited with Pt NPs for 5 min. Transmission spectra of GWF and Pt-GWF are shown in Fig. 4b. The deposition of Pt NPs reduced the sheet resistance of GWF (Fig. 4c) without significantly perturbing the transmittance of GWF. GWF and Pt-GWF was further characterized by Raman spectroscopy (Fig. 4d). The two prominent peaks in the Raman spectra represent the G-band (~1584 cm^{-1}) and the 2D-band (~2700 cm^{-1}). The 2D-band and G-band of GWF did not shift upon Pt deposition, similar to the result for multi-layer graphene deposited with Au NPs.[34] It is worth noting that when excessive Pt NPs were deposited on the GWF (Figs. S3a and S3b), the PCE of the cells declined. The *J-V* curve of the solar cell with excessive deposition of Pt NPs is shown in Fig. S3c. The decrease of the PCE was mainly caused by the reduced light transmittance due to the surface accumulation of Pt NPs.

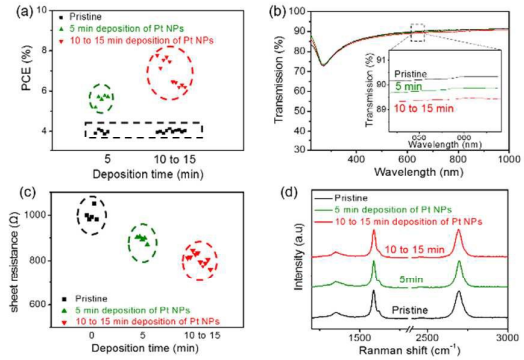

Figure 4. (a) PCEs of solar cells with different Pt NPs deposition time. (b) Transmission spectra of GWF and Pt-GWF with different Pt NPs deposition time. The inset shows the magnified region of 643 to 668 nm. (c) Sheet resistances of GWF and Pt-GWF with different Pt NPs deposition time. (d) Raman spectra of GWF and Pt-GWF with different Pt NPs deposition time.

Fig. 5 shows the UPS spectra of Ag, GWF/n-Si, and Pt-GWF/n-Si. The Fermi edge (E_{Fermi}) of Ag is same as that of GWF/n-Si and Pt-GWF/n-Si, as the Fermi edge is determined by the test condition. The right panel of Fig. 5a shows a zoomed-in view of the region near the Fermi edge for Ag and the E_{Fermi} is 21.68 eV. The right panel of Fig. 5b shows the secondary electron cut-off region of GWF/n-Si ($E_{GWF\text{-}Si\text{-}cutoff}$, 4.85 eV) and Pt-GWF/n-Si ($E_{Pt\text{-}GWF\text{-}Si\text{-}cutoff}$, 5.15 eV). The relationship among E_{cutoff}, E_{Fermi}, the energy of excitation source ($h\nu$, 21.22 eV), and the work function (Φ) is shown in Eq. (1).

$$\emptyset = h\nu + E_{\mathrm{Cutoff}} - E_{\mathrm{Fermi}} \quad (1)$$

According to Eq. (1), the work function of GWF/n-Si ($\Phi_{GWF\text{-}Si}$) and Pt-GWF/n-Si ($\Phi_{Pt\text{-}GWF\text{-}Si}$) was calculated as 4.39 eV and 4.69 eV, respectively. As the GWF did not fully cover the silicon wafer, the UPS measurement covered both the GWF and n-Si, resulting in a lower value of the work function of GWF/n-Si ($\Phi_{GWF\text{-}Si}$), compared to that of the work function of GWF (Φ_{GWF}). Hence, $\Phi_{GWF\text{-}Si}$ can be calculated as:

$$\emptyset = \frac{\emptyset_{n-Si} \cdot S_{n-Si} + \emptyset_C \cdot S_C}{S_{n-Si} + S_C} \quad (2)$$

where $\Phi_{C\text{-}Si}$ is the work function of coating/n-Si structure, $\Phi_{n\text{-}Si}$ is the work function of n-Si, $S_{n\text{-}Si}$ is the area of exposed n-Si, Φ_C is the work function of the coating materials, and S_C is the area of coating. The UPS spectra of n-Si and graphene were collected. As shown in Fig. S4a, the work function of n-Si ($\Phi_{n\text{-}Si}$) is 3.91 eV. The area ratio of GWF and n-Si is ~2.3 (Fig. S4c). According to Eq. (2), Φ_{GWF} is derived to be 4.60 eV, which is comparable to the work function of graphene (4.64 eV, Fig. S4b). In the self-deposition method, GWF was contacted with back electrode which caused more photoelectrons moving from back electrode to GWF. As the reduction process from $[PtCl_6]^{2-}$ to Pt occurred[28], more Pt NPs formed on the surface of GWF, suggesting that the major improvement of $\Phi_{Pt\text{-}GWF\text{-}Si}$ originated from the improvement of $\Phi_{Pt\text{-}GWF}$. The work function of Pt-GWF ($\Phi_{Pt\text{-}GWF}$) was calculated to be 5.03 eV. The improvement in Φ_{GWF} has a great influence on the Fermi level of GWF/n-Si. The energy band diagrams of GWF/n-Si and Pt-GWF/n-Si junctions are shown in Fig. 5c, d. The down-shifts of the Fermi level caused the increment of the barrier height and depletion region, which further influence the V_{oc} and J_{sc}.[9]

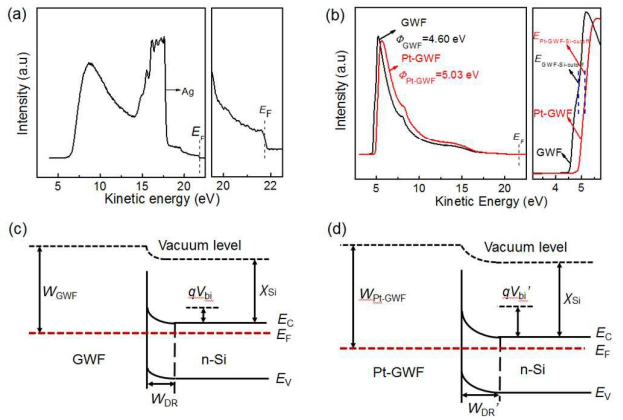

Figure 5. (a) UPS spectrum of Ag. The right panel shows the magnified region near Fermi edge. (b) UPS spectra of GWF/n-Si and Pt-GWF/n-Si. The right panel shows the secondary electron cut-off regions of GWF/n-Si and Pt-GWF/n-Si. (c) Energy band diagram of GWF/n-Si solar cell. (d) Energy band diagram of Pt-GWF/n-Si solar cell.

To further enhance the PCE of the Pt-GWF/n-Si solar cells, solid electrolyte (HNO_3+PVA) was coated on the Pt-GWF/n-Si surface to fabricate hybrid heterojunction and solid-state photoelectrochemical solar cells.[15] Fig. 6a shows the schematic diagram of a Pt-GWF/n-Si solar cell coated with solid electrolyte on the surface. Photoexcited charge carriers generated in n-Si are separated by the built-in field, where electrons are directed to the n-Si region and holes move toward the GWF (yellow arrows).[35] The n-Si and the redox

electrolyte also create a photoelectrochemical cell with the GWF counter electrode.

In a typical photochemical process, the holes driven to the n-Si surface are captured by NO^{3-} ions and diffuse to GWF, and then are further reduced back to NO^{3-}. This redox reaction forms a photoelectrochemical channel for charge carriers. Fig. 6b shows the energy diagram of the solid electrolyte coated Pt-GWF/n-Si solar cell in dark. The upper left part of Fig. 6b shows the energy diagram of the GWF/n-Si solar cell and the upper right part shows the photoelectrochemical solar cell. The barrier height of the photoelectrochemical solar cell is higher than that of the Pt-GWF/n-Si solar cell. The bottom right part of Fig. 6b shows the equilibrium energy diagram of the hybrid heterojunction and solid-state photoelectrochemical solar cell and the bottom left part of Fig. 6b shows the equilibrium energy diagram of the Schottky junction in this hybrid device. The barrier height between n-Si and solid electrolytes is equal to that between n-Si and Pt-GWF.

In this configuration, the two solar structures operate together in a parallel circuit, and the Schottky junction and photoelectrochemical effect work synergistically. In the hybrid heterojunction and solid-state photoelectrochemical solar cell, the solid electrolyte plays three roles simultaneously: an anti-reflection layer, a photoelectrochemical channel, and a chemical carrier.[15] As shown in Fig. 6c, after spin coating the solid electrolyte on the Pt-GWF/Si solar cell, the PCE was improved to 10.02%. In comparison, the efficiency of the solar cell which was only coated with solid electrolyte (without Pt NPs deposition) was 7.51%. The result suggests that that Pt NPs deposition significantly improved the performance of GWF/n-Si solar cells, and Pt NPs and HNO_3+PVA synergistically enhanced the PCE of GWF/n-Si solar cells.

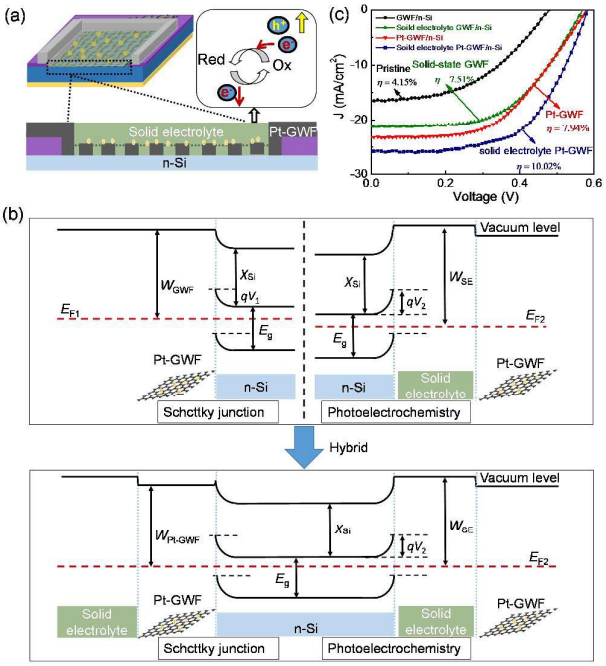

Figure 6. (a) Schematic diagram of the solid electrolyte coated Pt-GWF/n-Si solar cell (upper left), schematic diagram of electron transfer in the solid electrolyte (upper left), and the magnified region of the left panel (bottom). (b) Energy diagram of Pt-GWF/n-Si solar cell and photoelectrochemical solar cell in dark (Top panel), and energy diagram of the solid electrolyte coated Pt-GWF/n-Si solar cell in dark (Bottom panel). W_{GWF}, $W_{Pt\text{-}GWF}$ and W_{SE} are the work functions of GWF, Pt-GWF and solid electrolyte, respectively. E_g is the band gap of Si. X_{Si} is the electron affinity of Si. V_1, V_2 refer to the built-in potentials. E_{F1} and E_{F2} are the Fermi level of Pt-GWF/n-Si and photoelectrochemical solar cells in dark, respectively. (c) Light *J*-*V* curves of GWF/n-Si, Pt-GWF/n-Si, solid electrolyte coated GWF/n-Si and solid electrolyte coated Pt-GWF/n-Si solar cells.

Conclusions

In summary, we developed a practical and effective method to deposit Pt NPs on GWF to enhance the PCE of Pt-GWF/n-Si solar cells. The deposition of Pt NPs improved the work function of GWF without influencing the transmittance of GWF, and also decreased the sheet resistance of GWF. The increased work function of GWF resulted in an enhanced built-in electric field and thus an improved V_{OC}, while the enhanced conductivity led to a higher J_{SC}. After spin-coating solid electrolyte on the Pt-GWF/Si solar cell, the PCE of the resulting hybrid Schottky junction and photoelectrochemical solar cell was determined to be 10.02%, highest among all the GWF/n-Si solar cells developed in this study. However, it is worth noting that comparing with other metals, Pt is expensive. It is imperative to find a cheaper metal NPs to enhance the efficiency of graphene/Si solar cells in the future.

Acknowledgements

This work was supported by the National Science Foundation of China (51372133, 11374181), and Tsinghua National Laboratory for Information Science and Technology (TNList) Cross-discipline Foundation.

References

1 A. Geim, K. Novoselov, *Nat. Mater.*, 2007, **6**, 183.
2 X. Du, I. Skachko, A. Barker, E. Y. Andrei, *Nat. Nanotechnol.*, 2008, **3**, 491.
3 F. Bonaccorso, Z. Sun, T. Hasan, A. C. Ferrari, *Nat. Photonics,* 2010, **4**, 611.
4 Y. Song, X. Li, C. Mackin, X. Zhang, W. Fang, T. Palacios, H. Zhu, J. Kong, *Nano Lett.*, 2015, **15**, 2104.
5 E. Shi, H. Li, L. Yang, L. Zhang, Z. Li, P. Li, Y. Shang, S. Wu, X. Li, J. Wei, K. Wang, H. Zhu, D. Wu, Y. Fang, A. Cao, *Nano Lett.*, 2013, **13**, 1776.
6 X. Li, D. Xie, H. Park, T. H. Zeng, K. Wang, J. Wei, M. Zhong, D. Wu, J. Kong, H. Zhu, *Adv. Energy Mater.*, 2013, **3**, 1029.
7 Y. Ye, L. Dai, *J. Mater. Chem.*, 2012, **22**, 24224.
8 L. Lancellotti, T. Polichetti, F. Ricciardella, O. Tari, S. Gnanapragasam, S. Daliento, G. D. Francia, *Thin Solid Films*, 2012, **522**, 390.
9 Y. Shi, K. K. Kim, A. Reina, M. Hofmann, L. Li, J. Kong, *ACS Nano*, 2010, **4**, 2689.
10 X.M. Li, Z. Lv, H.W. Zhu, *Adv. Mater*. 2015, **27**, 6549.
11 P. Ho, Y. Liou, C. Chuang, S. Lin, C. Tseng, D. Wang, C. Chen, W. Hung, C. Wen, C. Chen, *Adv. Mater.*, 2015, **27**, 1724.
12 X. Li, D. Xie, H. Park, M. Zhu, T. H. Zeng, K. Wang, J. Wei, D. Wu, J. Kong, H.Zhu, *Nanoscale*, 2013, **5**, 1945.

13 X. Miao, S. Tongay, M. K. Petterson, K. Berke, A. G. Rinzler, B. R. Appleton, A. F. Hebard, *Nano Lett.*, 2012, **12**, 2745.
14 L. Yang, X Yu. M. Xu, H. Chen, D. Yang, *J. Mater. Chem. A*, 2014, **2**, 16877.
15 X. Li, X. Zang, X. Li, M. Zhu, Q. Chen, K. Wang, M. Zhong, J. Wei, D. Wu, H. Zhu, *Adv. Energy Mater.*, 2014, **4**, 1400224.
16 X. Li, P. Sun, L. L. Fan, M. Zhu, K. Wang, M. Zhong, J. Wei, D. Wu, Y. Cheng, H. Zhu, *Sci. Rep.*, 2012, **2**. 395.
17 X. Liu, Z X. W. hang, J. H. Meng, Z. G. Yin, L. Q. Zhang, H. L. Wang, J. L. Wu, *Appl. Phys. Lett.*, 2015, **106**, 233901.
18 Y. Lin, X. Li, D. Xie, T. Feng, Y. Chen, R. Song, H. Tian, T. Ren, M. Zhong, K. Wang, H. Zhu, *Energy Environ. Sci.*, 2013, **6**, 108.
19 Y. F. Li, W. Yang, Z. Q. Tu, Z. C. Liu, F. Yang, L. Q.Zhang, R. Hatakeyama, *Appl. Phys. Lett.*, 2014, **104**, 43903.
20 Y. Song, X. Li, C. Mackin, X. Zhang, W. Fang, T. Palacios, H. Zhu, J. Kong, *Nano Lett.*, 2015, **15**, 2104.
21 T. Feng, D. Xie, Y. Lin, Y. Zang, T. Ren, R. Song, H. Zhao, H. Tian, X. Li, H. Zhu, L. Liu, *Appl. Phys. Lett.* 2011, **99**, 233505.
22 X. Zhang, C. Xie, J. Jie, X. Zhang, Y. Wu, W. Zhang, *J. Mater. Chem. A*, 2013, **1**, 6593.
23 C. Xie, X. Zhang, K. Ruan, Z. Shao, S. S. Dhaliwal, L. Wang, Q. Zhang, X. Zhang, J. Jie, *J. Mater. Chem. A*, 2013, **1**, 15348.
24 V. V. Brus, M. A. Gluba, X. Zhang, K. Hinrichs, J. Rappich, N. H. Nickel, *Phys. Status Solidi A*, 2014, **211**, 843.
25 H. Liu, Y. Liu, D. Zhu, *J. Mater. Chem. A*, 2010, **21**, 3335.
26 A. Bragaru, E. Vasile, C. Obreja, M. Kusko, M. Danila, A. Radoi, *Mater. Chem. Phys.*, 2014, **146**, 538.
27 S. Shironita, K. Mori, T. Shimizu, T. Ohmichi, N. Mimura, H. Yamashita, *Appl. Surf. Sci.*, 2008, **254**, 7604.
28 D. Zhang, W. C. Chang, T. Okajima, T. Ohsaka, *Langmuir*, 2011, **27**, 14662.
29 P. Zhai, Y. Chang, Y. Huang, T. Wei, H. Su, S. Feng, *Electrochim. Acta*, 2014, **132**, 186.
30 Z. Li, P. Zhang, K. Wang, Z. Xu, J. Wei, L. Fan, D. Wu, H. Zhu, *J. Mater. Chem.*, 2011, **21**, 13241.
31 H. A. Atwater, A. Polman. *Nat. Mater.*, 2010, **9**, 205.
32 N. V. Long, N. D. Chien, T. Hayakawa, H. Hirata, G. Lakshminarayana, M. Nogami, *Nanotechnol.*, 2010, **21**, 35605.
33 M. Yen, C. Teng, M. Hsiao, P. Liu, W. Chuang, C. Ma, C. Hsieh, M. Tsai, C. Tsai, *J. Mater. Chem.*, 2011, **21**, 12880.
34 K. K. Kim, A. Reina, Y. Shi, H. Park, L. J. Li, Y. H. Lee, J. Kong, *Nanotechnol.*, **2010**, 21, 285205.
35 Q. K. Shu, J. Q. Wei, K. L. Wang, H. W. Zhu, Z. Li, Y. Jia, X. C. Gui, N. Guo, X. M. Li, C. R. Ma, D.H. Wu, *Nano Lett.*, 2009, **12**, 4338.